Catalysis Science & Technology

PAPER

View Article Online
View Journal | View Issue

Cite this: *Catal. Sci. Technol.*, 2016, **6**, 4168

The effect of gold on modern bimetallic Au–Cu/MWCNT catalysts for the oxy-steam reforming of methanol

Pawel Mierczynski,*[a] Krasimir Vasilev,[b] Agnieszka Mierczynska,[c] Waldemar Maniukiewicz,[a] Radoslaw Ciesielski,[a] Jacek Rogowski,[a] Iwona M. Szynkowska,[a] A. Yu. Trifonov,[d] Sergey V. Dubkov,[d] Dmitry G. Gromov[d] and Tomasz P. Maniecki[a]

Received 1st October 2015,
Accepted 7th January 2016

DOI: 10.1039/c5cy01667c

www.rsc.org/catalysis

Copper and gold doped copper catalysts supported on multi-walled carbon nanotubes were prepared by wet impregnation and deposition–precipitation methods, respectively. The catalysts were tested in the oxy-steam reforming of methanol (OSRM) and characterized by XRD, SEM-EDS, TOF-SIMS, thermo-gravimetric analysis and temperature-programmed desorption of ammonia. The reactivity results showed the promotion effect of gold on the activity and selectivity of the copper catalysts in the OSRM. The formed Cu–Au alloy as an active phase was responsible for the activity and selectivity improvement of the bimetallic catalysts in the oxy-steam reforming of methanol. The formation of an Au–Cu alloy was confirmed by the XRD, TOF-SIMS and SEM-EDS techniques. The reducibility and acidity of the tested catalysts are important factors, which influence the activity of the copper and gold–copper catalysts.

Introduction

Hydrogen fuel cells enable the generation of electric energy in an ecologically clean way. The use of fuel cells instead of the traditional methods could reduce carbon dioxide emissions by 40%–60% and nitrogen oxide emissions by 50%–90%, which is expected to have a significant impact on the environment. Hydrogen is also an ideal fuel for every means of transport (cars, railways, ships and space ships) because it is utilized without environmental contamination and the only waste product is water.

An attractive solution to problems associated with storing molecular hydrogen involves the catalytic production of hydrogen from a high-energy liquid fuel such as methanol.[1]

Hydrogen can be synthesized as a result of the catalytic reforming of methanol, partial oxidation of methanol or oxy-steam reforming of methanol. The thermodynamics of the partial oxidation and steam reforming of methanol suggests that the most energetically favourable solution is a combination of these two reactions in one process. Heat accompanying the oxy-steam reforming of methanol is sufficient to run this autothermal reaction, which enables utilization in applications (*e.g.* fuel cells) and improves the economics of the hydrogen fusion process.[2] Depending on the reagent stoichiometry, the reactions take place according to the following equations: oxidation of methanol:

$$CH_3OH + 0.5\ O_2 \leftrightarrow CO_2 + 2\ H_2 \quad \Delta H^\circ = -192.2\ \text{kJ mol}^{-1}$$

$$CH_3OH + 0.25\ O_2 \leftrightarrow 0.5\ CO_2 + 0.5\ CO + 2H_2\ \Delta H^\circ = -50.8\ \text{kJ mol}^{-1}$$

steam reforming of methanol:

$$CH_3OH + H_2O \leftrightarrow CO_2 + 3H_2 \quad \Delta H^\circ = 49.7\ \text{kJ mol}^{-1}$$

oxy-steam reforming of methanol:

$$CH_3OH + 0.25\ O_2 + 0.5\ H_2O \leftrightarrow CO_2 + 2.5\ H_2 \quad \Delta H^\circ = -71.4\ \text{kJ mol}^{-1}$$

The oxy-steam reforming of methanol is a promising method for hydrogen generation because it can be conducted under

[a] *Institute of General and Ecological Chemistry, Lodz University of Technology, Zeromskiego 116, 90-924 Lodz, Poland. E-mail: pawel.mierczynski@p.lodz.pl, mierczyn25@wp.pl; Fax: 0048 42 631 31 28; Tel: + 48 42 631 31 24*
[b] *Mawson Institute, University of South Australia, Mawson Lakes SA 5095, Adelaide, Australia*
[c] *The Australian Wine Research Institute, Waite Precinct, Hartley Grove cnr Paratoo Road, Urrbrae (Adelaide), SA 5064, Australia*
[d] *National Research University of Electronic Technology (MIET), pr. 4806 5, Zelenograd, Moscow, 124498 Russia*

atmospheric pressure and in a low temperature range (T = 150–350 °C). Furthermore, this is an autothermal process, which does not require supplying any externally added energy to run. This provides opportunities to generate hydrogen in a place where it is needed. The problem is to obtain pure hydrogen (without carbon monoxide)[3] which can be used directly to power fuel cells. Carbon monoxide is formed during methanol decomposition, which runs at a higher temperature during the oxy-steam reforming process.

The typical catalysts used in the reforming of methanol are Cu, Ni, Co, Fe, Pd, Pt, Ru, Au, Ir, and Ag supported on mono-Al_2O_3, ZnO, CeO_2, MgO, La_2O_3, SiO_2,[4–8] and binary oxides such as ZnO–Al_2O_3, CeO_2–ZrO_2, SiO_2–SnO_2, and Al_2O_3–CeO_2.[7–10] These catalytic systems are prepared using different methods including microemulsion,[11] aerogel,[12] coprecipitation,[13] sol–gel,[14] impregnation[15] and combustion synthesis. The most common catalysts used for the methanol reforming reaction are the copper supported catalysts. High values of copper dispersion, metal surface area, along with a small particle size, are the targets to attain highly active catalysts. Numerous published reports deal with the addition of promoters[10,16–19] and the influence of the preparation method[2,13,20,21] on the catalytic properties of the copper supported catalysts are examined. Despite the high activity and selectivity of copper catalysts such as CuO/ZnO, CuO/ZnO/Al_2O_3 in the methanol oxidation reaction, there are still ongoing issues concerned with their yield, selectivity and enhancement of their stability.[22]

In the past decades there has been increased interest in catalysts supported on gold. This is mainly based on the pioneering report of Haruta *et al.* which showed the high activity of gold nanoparticles supported on TiO_2 or Fe_2O_3 oxides in the oxidation reaction of carbon monoxide carried out at low temperature.[23] Since then, gold supported catalysts have been tested in a number of chemical processes such as the low temperature conversion of methane with water vapour, conversion of carbon monoxide with water vapour (WGS),[24] hydrogenation and dehydrogenation reactions,[24–27] oxidation of CO,[28] selective oxidation of hydrocarbons[29,30] and selective oxidation of alcohols and aldehydes in fuel cell technology and in pollution control.

Furthermore, we decided to promote the copper catalysts supported on MWCNTs by gold because of its well-known CO oxidation activity.[31] The literature data regarding the reforming of methanol have confirmed the high activity of gold catalysts and they have shown a low selectivity towards the formation of carbon monoxide.[32–35]

Bimetallic Au–Cu catalysts have shown high activity in various reactions due to the alloy formed, which is the active phase compared to the individual Au and Cu catalysts. The classification of the Au–Cu alloy depends strongly on the origin of the CuO species which could be highly dispersed, bulky types and/or on the oxidation states of the Cu species (Cu^{2+}, Cu^{+}, and Cu^{0}).[32]

While there are a handful of publications concerned with Cu/CNT[36,37] catalysts in the steam reforming of methanol, there are no published papers that report the role of bimetallic Au–Cu/CNT catalysts in hydrogen production.

To fill this gap, we investigate the potential of bimetallic Au–Cu catalysts deposited on carbon nanotubes in the oxy-steam reforming of methanol. The selection of the active phase components for the catalysts used in this work (Cu, Au) was based on their reactivity, both in relation to hydrogen, as well as carbon monoxide (unwanted reaction product). The well-known copper catalysts supported on a metal oxide are highly active in the reforming of methanol reaction.[22,38] However, copper catalysts do not exhibit satisfactory selectivity and stability in the methanol reforming reaction. One way to increase the selectivity and stability of the catalyst system is by the promotion of a copper catalyst by introduction of a small amount of a noble metal. The ideal promoter which increases the activity, selectivity and stability in many catalytic processes is gold as evidenced by the number of reports in the literature concerning gold catalysts.[24,26,30,32,39–46]

The main advantages of using carbon nanotubes (CNTs) as a catalyst support are their high purity, high thermal and mechanical stability, occurrence of specific interaction on the support–metal boundary, adsorption of catalytically active nanoparticles on the external wall of CNTs, and the CNT electron structure. CNTs with good conductivity are also proposed to promote the spillover effect. Additionally, the possibility of introducing functional groups into the surface of the carbon nanotubes allows tuning the sorption properties of the resulting nanomaterial. All these features of carbon nanotubes have a huge impact on the activity and selectivity of catalysts supported on CNTs.[47–53] The choice of carrier material has been dictated by the special properties of carbon nanotubes which could provide an ideal material for electrodes used in fuel cell technology. In addition, this work proved that gold–copper catalysts supported on multi-walled carbon nanotubes (MWCNTs) allow to achieve a high yield of hydrogen production in parallel with a high content of carbon monoxide in the reaction product. Carbon monoxide can be oxidized in the next step to carbon dioxide, which makes these catalytic systems possible for use in fuel cell technology. The high activity of such systems can lead to the replacement of platinum electrodes since they exhibit superior activity in the presence of a high content of carbon monoxide in a product mixture.

The specific aims of this work are to determine the effect of gold on the physicochemical properties and catalytic reactivity of copper supported catalysts in the oxy-steam reforming of methanol and to correlate the physicochemical properties of the prepared systems with their catalytic activity in the oxy-steam reforming of methanol. The monometallic copper and bimetallic Au–Cu/MWCNT supported catalysts were prepared by a wet aqueous impregnation method and a deposition–precipitation method, respectively. Their physicochemical properties were investigated using thermogravimetric analysis (TG), X-ray diffraction (XRD), temperature-programmed reduction (TPR-H_2), TOF-SIMS, SEM-EDS and temperature-programmed desorption of

ammonia (TPD-NH_3) methods. Catalytic activity tests in the oxy-steam reforming of methanol were carried out using a fixed bed quartz microreactor under atmospheric pressure in the temperature range of 200–300 °C.

Experimental

Preparation of catalysts

2.1.1 Preparation of the monometallic copper catalysts. Metal phase Cu was introduced on the multi-walled carbon nanotube surface (MWCNT – purchased from Sigma-Aldrich CAS: 308068-56-6) by using a wet impregnation method using aqueous solutions of copper nitrate. The supported catalysts were then dried for 2 h at 120 °C and calcined for 4 h in air at 350 °C.

2.1.2 Preparation of the bimetallic gold–copper supported catalysts. The gold phase was introduced into the monometallic copper catalyst surface prepared by using a deposition–precipitation method described elsewhere.[54]

In the first stage of the preparation of the bimetallic supported catalysts, an aqueous solution of chloroauric acid was added into the solution containing the suspended Cu/MWCNT catalyst which was calcined in an air atmosphere at 350 °C for 4 h. The resulting solution was stirred at 65 °C. In the next step, urea was used to achieve a pH value of 8. The gold loading on the catalyst was 1 wt%. After aging for two hours, the precipitate was filtered and washed with hot water until no chloride ions were detected using a 0.1 M $AgNO_3$ solution. Then, the resulting precipitate was dried overnight in air at 80 °C, and afterwards it was calcined at 180 °C for 4 h in an air atmosphere. The copper and gold or nickel and gold loadings were 20 wt% and 0.5, 1, 5 wt%, respectively.

Characterization of the catalysts

2.2.1. Thermogravimetry/differential thermal analysis (TG/DTA). TG/DTA analysis, performed on a Derivatograph Type: 34-27T (MOM, Budapest), was used for the temperature programmed decomposition of the nanomaterials including the multi-walled carbon nanotubes and the mono- and bimetallic Au–Cu catalysts in an air atmosphere. The TG-DTA measurements were carried out applying a sample weight of about 50 mg in a linear heating rate of 10 °C min^{-1} and a temperature range of 25–1000 °C.

2.2.2. Temperature-programmed reduction (TPR-H_2). The TPR-H_2 measurements were carried out in an automatic TPR system AMI-1 in the temperature range of 25–900 °C with a linear heating rate of 10 °C min^{-1}. The samples (weight about 0.1 g) were reduced in a hydrogen stream (5% H_2–95% Ar) with a volumetric flow rate of 40 cm^3 min^{-1}. A thermal conductivity detector monitored the hydrogen consumption.

2.2.3. Temperature-programmed desorption of ammonia (TPD-NH_3). The TPD-NH_3 measurements were carried out in a quartz reactor using NH_3 as a probe molecule. NH_3 was adsorbed on the samples at 50 °C for 30 min after purification of the catalyst surface in flowing He at 600 °C for 60 min. The temperature-programmed desorption of NH_3 was carried out in the temperature range of 100–600 °C using a linear temperature growth rate (25 °C min^{-1}) and a thermal conductivity detector, after removing the physisorbed ammonia from the sample surface.

2.2.4. X-ray diffraction (XRD) measurements. The room temperature powder X-ray diffraction patterns were collected using a PANalytical X'Pert Pro MPD diffractometer in the Bragg–Brentano reflection geometry. Copper CuK_α radiation from a sealed tube was used. Data were collected in the 2θ range of 5–90° with a step of 0.0167° and exposure per step of 27 s. Due to the fact that the raw diffraction data contain some noise, the background during the analysis was subtracted using the Sonneveld, E. J. and Visser algorithm. The data were then smoothed using a cubic polynomial. All calculations were done using the X'Pert HighScore Plus computer software.

XRD "*in situ*" measurements

Approximately 150 mg of the sample, which had been ground in an agate mortar, was packed in a glass ceramic (Macor) sample holder. The gas mixture 5% H_2–95% Ar was used as a reducing reagent for the 5% Au–20% Cu/MWCNT catalyst. The sample was heated at a nominal rate of 2 °C min^{-1}. The high-temperature wide-angle X-ray diffraction data were collected using a PANalytical X'Pert Pro diffractometer equipped with an Anton Paar XRK900 reactor chamber, using every 50 °C interval starting from 50 °C and ending at 800 °C. A PANalytical X'Celerator detector based on Real Time Multiple Strip technology capable of simultaneously measuring the intensities in the 2θ range of 10–90° was used.

2.2.4. SEM-EDS measurements. The SEM measurements were performed using a Hitachi S-4700 scanning electron microscope (Japan), equipped with an energy dispersive spectrometer (EDS, Thermo Noran, USA). Images were recorded at several magnifications using a secondary electron or a BSE detector. The EDS method made it possible to determine the qualitative analysis of elements present in the studied micro-area of the sample surface layer on the basis of the obtained characteristic X-ray spectra. A map of the distribution of elements on the studied micro-area was made. The accelerating voltage was 25 kV. For the analysis, the samples were coated with a carbon target using a Cressington 208 HR system.

2.2.5. TOF-SIMS analysis. The secondary ion mass spectra were recorded using a TOF-SIMS IV mass spectrometer manufactured by Ion-Tof GmbH, Muenster, Germany. The instrument is equipped with a Bi liquid metal ion gun and a high mass resolution time of flight mass analyzer. The secondary ion mass spectra were recorded from an approximately 100 μm × 100 μm area of the spot surface. During measurement the analysed area was irradiated with pulses of 25 keV Bi^{3+} ions at a 10 kHz repetition rate and an average ion current of 0.5 pA. The analysis time was 30 s for both negative secondary ions giving an ion dose below the static

limit of 1×10^{13} ions cm^{-2}. The secondary ions emitted from the bombarded surface were mass separated and counted in the time of flight (TOF) analyzer.

2.3 Catalytic activity tests

The oxy-steam reforming of methanol (OSRM) was performed using a flow quartz reactor under atmospheric pressure. The reaction was carried out at two temperatures, 200 and 300 °C, respectively. HPLC grade methanol (Aldrich, water ~0.03 wt%) was used. The catalyst loading was 0.1 g and the stream composition was: $H_2O/CH_3OH/O_2$ = 1/1/0.4 (molar ratio) and the GHSV was 26 700 h^{-1} (calculated at ambient temperature and under atmospheric pressure). The total flowrate was kept at 31.5 ml min^{-1} and the Ar was used as the balance gas (the methanol content in the reaction mixture was 6%). All the catalysts before the activity test were reduced "*in situ*" at 300 °C in a mixture of 5% H_2–95% Ar for 1 h. The steady-state activity measurements at each temperature were taken after at least 2 h in the stream. The analysis of the reaction organic products (methanol, methane, methyl formate, dimethyl ether (DME), and formaldehyde) was carried out by using an on-line gas chromatograph equipped with an FID and a 10% Carbowax 1500 on a Graphpac column. The CO, CH_4 and CO_2 concentrations were monitored by a GC chromatograph equipped with a TCD (150 °C, 60 mA) and a Carbosphere 60/80 (50 °C) column. The hydrogen concentration was measured by a GC chromatograph equipped with a TCD (120 °C, 60 mA) and a Molecular Sieve 5a (120 °C) column. The material balances on carbon were calculated to verify the obtained results. The selectivity towards the formation of hydrogen, carbon monoxide or carbon dioxide in the OSRM was calculated using eqn (1),[22] (2), and (3) and the conversion of methanol using eqn (4):[22]

$$Y_{H_2}(\%) = \frac{nH_{2-out}}{n_1^{in}\ CH_3OH - n_2^{out}\ CH_3OH} \quad (1)$$

$$S_{CO}(\%) = \frac{(nCO_{out})}{\sum \text{carbon-containing products}} \times 100 \quad (2)$$

$$S_{CO_2}(\%) = \frac{(nCO_{2\text{-}out})}{\sum \text{carbon - containing products}} \times 100 \quad (3)$$

where, nCH_3OH and nH_2 are the molar flow rates of CH_3OH and H_2, respectively.

$$\text{Conv.}_{CH_3OH} = \frac{n_1^{in}\ CH_3OH - n_2^{out}\ CH_3OH}{n_1^{in}\ CH_3OH} \times 100 \quad (4)$$

where:

nH_{2-out} – the molar flow rate of the H_2 feed out,

nCO_{2-out} – the molar flow rate of the CO_2 feed out,

nCO_{out} – the molar flow rate of the CO feed out,

$nDME_{out}$ – the molar flow rate of the DME feed out,

$n_1^{in}CH_3OH$, $n_2^{out}CH_3OH$ – the molar flow rates of the CH_3OH feed in and feed out, respectively.

3. Results and discussion

3.1 Thermo-gravimetric TG analysis

The influence of copper and/or gold on the thermal decomposition of the MWCNTs was investigated by the thermal decomposition studies. The results from the TG analysis carried out in the temperature range of 25–1000 °C for the multi-walled carbon nanotubes, mono and bimetallic supported catalysts are given in Fig. 1. The thermal decomposition process of the MWCNTs starts at 520 °C and ends at 980 °C. The decomposition process proceeds in two steps: the first step is associated with water and impurity removal and takes place in the temperature range of 30–200 °C. This is evident in the changes in the TG and DTG curves associated with the endothermic DTA peak situated in the temperature range of 30–200 °C. The second step is related to the oxidation of the multi-walled carbon nanotubes directly to carbon dioxide as evident in the DTA curve in the temperature range of 520–980 °C. Mosquera *et al.*[55] studied the CNT purity based on thermo-gravimetric analysis (TGA) of an 'as grown' sample from room temperature to 800 °C at 10 °C min^{-1}. The TG results showed that an initial weight loss of around 0.20–0.25% in the temperature range of 60–100 °C was due to the removal of the volatile organic impurities while the thermal degradation of the CNTs began in the temperature range of 567–689 °C (depending on the synthesis conditions) and was completed around 800 °C. The TGA weight loss confirmed the 96% purity of the investigated nanomaterial. Mosquera *et al.*[55] have also found that the presence of impurities, *e.g.* metal, has a significant influence on the thermal stability. A high temperature oxidation of CNTs indicates a low degree of graphitisation, and the presence of many defects and disorder.

The thermal analysis of the copper catalysts also showed the decomposition of the Cu/MWCNT to be a two-stage process. The differences in the thermal decomposition studies between the multi-walled carbon nanotubes and the monometallic copper catalysts were the starting and ending decomposition temperatures observed for these two samples. The oxidation of the multi-walled carbon nanotubes in the case of the 20% Cu/MWCNT supported catalyst took place in the temperature range of 470–760 °C, whereas for the bare MWCNTs this process is in the 520–980 °C temperature

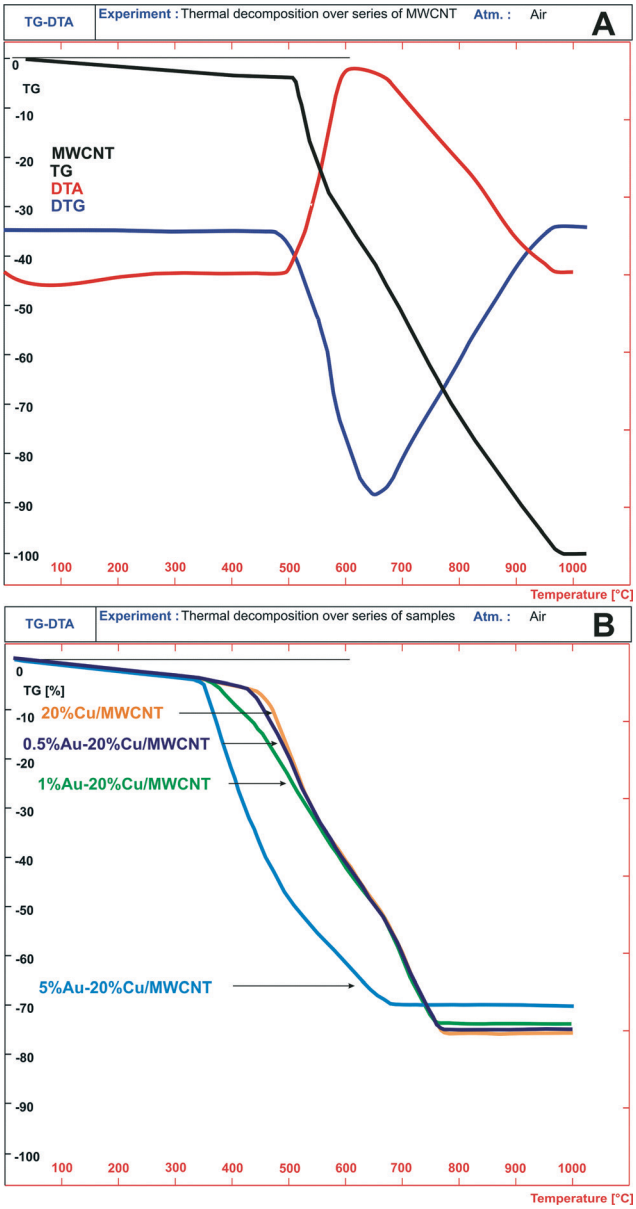

Fig. 1 A) TG-DTA curves of the pristine MWCNTs, B) TG curves recorded for the monometallic supported catalysts, 20% Cu/MWCNT, and the bimetallic catalysts 0.5% Au–20% Cu/MWCNT, 1% Au–20% Ni/MWCNT, and 5% Au–20% Cu/MWCNT obtained during the temperature programmed decomposition process performed in an air atmosphere.

range. The promotion of the monometallic copper supported catalysts by gold resulted in a further decrease of the initial oxidation temperature of the nanomaterial. The higher the gold loading level was, the lower was the decomposition temperature of the oxidation process of the carbon nanotubes. For the catalyst containing 0.5% wt gold, the initial oxidation temperature was 420 °C, whereas for the catalysts with a higher gold content of 1 and 5% wt, the temperature increased to 370 and 350 °C, respectively. No significant promotion effect of gold addition on the monometallic copper supported catalysts on the final decomposition temperature was observed, for which the final temperature of decomposition was 760 °C. The only exception was the final decomposition temperature recorded for the catalyst with the highest gold content (5% wt Au), which reached 690 °C. The TG, DTG and DTA data for all the investigated catalytic systems confirmed the obtained results.

3.2. The effect of gold on the reduction behavior of the Cu/MWCNT catalysts

The H_2-TPR technique was used to illustrate the reducible properties of the mono- and bimetallic catalysts supported on the multi-walled carbon nanotubes and the results are given in Fig. 2.

While the reduction of the carbon nanotubes showed that the nanomaterial itself is irreducible in the investigated temperature range, the TPR profile of the Cu/αAl_2O_3 system (prepared by an impregnation method and calcined at 400 °C) demonstrated that the incorporated copper oxide is reduced in a single reduction stage situated at 250–350 °C.

In the next stage of the reduction studies, we carried out the reduction of the 20% Cu catalysts supported on MWCNTs. The results showed two unresolved reduction profiles visible in the temperature range of 150–380 °C attributed to the two-step reduction of the copper(II) oxide *via* the intermediate Cu_2O (named the LT-peak (220 °C) and the HT-peak (300 °C), accordingly). Additionally, the third wide high temperature desorption stage, seen in the TPR profile in the temperature range of 390–800 °C, is assigned to the methanation process of the MWCNTs.[56,57]

Mahata *et al.*[58] also investigated the reduction behavior of a copper catalyst supported on MWCNTs. The authors observed a single reduction peak in the temperature range of 180–375 °C, with the maximum of the hydrogen consumption peak situated at 250 °C.

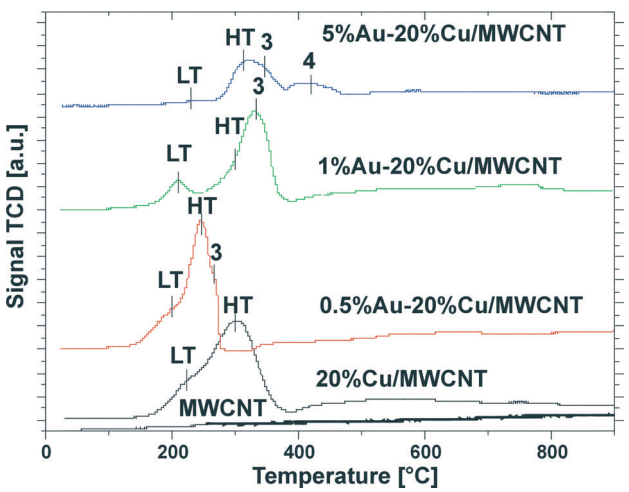

Fig. 2 TPR profile of the pristine MWCNTs, the monometallic copper catalyst after calcination in air for 4 h at 350 °C and the bimetallic Au–Cu catalysts after calcination in air for 4 h at 180 °C.

The reduction of the CuO/CNT catalysts was studied by Song *et al.*[59] using the H_2-TPR technique. The authors observed only one reduction stage coming from the reduction of the CuO species in the range of 100–300 °C and did not observe any peak corresponding to the reduction of pristine CNTs. Furthermore, their results suggested that the reduction temperature of the CuO nanoparticles has a strong dependence on the defect density of the CNT material. They claimed also that the defects might promote electron transfer during the reduction process which destabilizes the bonds between copper and oxygen and thereby facilitates the reduction of CuO to metallic Cu.

The reduction behavior of copper catalysts supported on CNT was also investigated by Groβmann *et al.*[60] The authors observed one reduction effect on the TPR profile, which is connected with the reduction of CuO to metallic copper with the maximum of the hydrogen consumption peak situated at 176 °C. The shape of the TPR profile with a small shoulder at low temperatures pointed out the presence of two copper oxide particle sizes on the catalyst surface.

Introduction of 0.5% wt gold into the monometallic copper supported catalyst caused a shift of the reduction effect to the lower temperature region, which confirms that the addition of gold facilitates the reduction of the copper oxide species.[61] The TPR-H_2 profile recorded for 0.5% Au–20% Cu/MWCNT showed four partially resolved reduction peaks associated with the reduction of the catalytic material and the methanation process of the carbon nanotubes. The first peak (LT-peak) with the maximum of the hydrogen consumption peak at 205 °C is assigned to the CuO to Cu_2O reduction. The second visible peak with the maximum of the hydrogen consumption situated at 245 °C (HT-peak) is associated with the reduction of Cu_2O to metallic copper. The third faintly resolved reduction peak with the maximum of the hydrogen consumption at 265 °C is attributed to the reduction of the copper oxychloride species ($Cu_2(OH)_3Cl$). The last wide peak located in the high temperature range of 360–800 °C is assigned to the methanation process of the MWCNTs.

Copper(II) oxide reduction as a result of gold promotion is explained in published reports by the spillover phenomenon between copper oxide and metallic gold.[61–64] The shifts of the low temperature reduction stage towards lower temperatures in the TPR-H_2 profile of the AuCu/TiO_2 catalyst were also observed by Chimentão *et al.*[65] This was explained by the electronic interaction between the Au and Cu atoms. An electron transfer from copper to metallic gold results in a lower reduction temperature of the observed TPR-H_2 peak. In resonance with our studies, an alloy formation was confirmed using the XRD, XPS and transmission microscopy techniques. They have found that the alloy particle size decreases with an increase in the copper content in the catalyst system.

The confirmation of the alloying process which takes place between gold and copper is the shift of the observed effects associated with the copper oxide species reduction in the case of the bimetallic catalyst towards the lower temperature range in comparison to the effects observed for the monometallic copper catalyst. The same behavior was observed in the case of the 0.5% Au–20% Cu/MWCNT catalysts. In addition, in the case of the 0.5% Au–20% Cu/MWCNT catalyst the high temperature effect located in temperature range of 390–800 °C was visible in the TPR-H_2 profile. The effect is also attributed to the same effect observed for the monometallic copper catalyst[56] and it can be also associated with the desorption of the hydrogen chloride from the carbon material.[57]

The same spillover effect was postulated for the bimetallic Cu–Ni/ZrO_2 catalyst[64] based on the shift of the observed low temperature reduction peak towards lower temperatures. In addition, this shift has suggested the reduction of the adjacent Cu and Ni atoms, which leads to the bimetallic phase. The formation of the bimetallic CuNi particles was detected by the HREM-TEM-EDX technique.

Pongstabodee *et al.*[66] studied the reduction properties of the monometallic Au and Cu and bimetallic Au–Cu catalysts supported on CeO_2. The authors have found that Au facilitated copper oxide reduction and caused a shift of the reduction peaks to a lower temperature range. They also claimed that the Au/CuO–CeO_2 catalysts are reduced in two steps. CuO is firstly reduced to Cu^+ at low temperature and then Cu^+ is reduced to metallic copper.

Similar findings were postulated by Yang *et al.*[67] who also studied the reduction behavior of copper, gold and gold–copper catalysts supported on zinc oxide. The results showed that the TPR-H_2 profile recorded for the gold supported catalyst did not show any reduction stage. This indicated that gold was present only in a metallic state after calcination at 573 K or the gold oxide crystallite size was too small to be detected by XRD. The reduction pattern of the copper catalyst supported on ZnO showed three reduction stages: a major peak situated at about 500 K and two smaller shoulders located at 460 and 525 K, respectively. The major peak was assigned to the reduction of CuO to metallic copper, while the shoulder at 460 K was attributed to the CuO to Cu^+ reduction stage and the high temperature shoulder was assigned to the reduction of the Cu^+ species to Cu^0.[68,69] On the other hand, the TPR-H_2 profile of the Au/CuO/ZnO sample showed two unresolved reduction peaks at 486 and 500 K which were assigned to the two step reduction (Cu(II)→Cu(I)→Cu(0)). It is worth to note that the reduction stage of CuO in the Au/CuO/ZnO catalyst was shifted to a lower temperature compared with the CuO/ZnO catalyst. This result confirmed that Au promotes CuO reduction. The enhanced reducibility of CuO in the case of the catalyst promoted by Au is explained by the weak Cu–O bond due to the metallic gold. The authors suggested that there is some sort of interaction between metallic gold and copper(II) oxide in the case of the Au/CuO/ZnO system.

The reduction profile of the 1% Au–20% Cu/MWCNT catalyst shows four effects. The first three of these are associated with the reduction of the copper containing species. The first reduction stage with the maximum of the hydrogen consumption peak located at about 210 °C is assigned to the

reduction of CuO to Cu_2O. The second profile situated at 300 °C is attributed to the Cu_2O species reduction, while the third reduction peak with the maximum of the hydrogen consumption located at 330 °C is assigned to the copper oxychloride species ($Cu_2(OH)_3Cl$) reduction. The precise description of the third step of the reduction was given in our previous work.[57] The last wide peak visible on the TPR curve located in the temperature range of 390–800 °C is assigned to the carbon nanotube methanation process[56] and it can be also associated with the desorption of the hydrogen chloride from the carbon material.[57]

Increasing the gold content to 5% wt has caused changes in the reduction behavior of the bimetallic Au–Cu catalyst. The formation of the four reduction stages in the TPR profile of this catalyst was observed. The first wide reduction stage visible in the temperature range of 180–280 °C is assigned to the CuO reduction. The second reduction peak with the maximum of the hydrogen consumption peak located at 325 °C is attributed to the Cu_2O species reduction. The third reduction effect with the maximum of the hydrogen consumption peak located at about 350 °C is assigned to the copper(II) oxychloride species reduction.[57] Lastly, the fourth reduction stage is attributed to the copper(II) chloride reduction. Also, in the case of the 5% Au–20% Cu/MWCNT system the fifth effect was visible in the TPR-H_2 profile. This effect was associated with both the methanation process of the MWCNTs and the desorption of hydrogen chloride from the carbon material.[57]

The temperature-programmed reduction (H_2-TPR) data for both the monometallic copper and bimetallic Au–Cu/MWCNT supported catalysts are given in Table 1. The temperature maxima and the contribution of each peak to the overall TPR peak area are also presented in this table. From the data presented in the table, it is easy to observe that the copper catalyst promoted by the lowest gold content is reduced at the lowest temperature range compared to the other systems. The low temperature reduction peaks gave evidence that from these copper oxide species: 1. metallic copper crystallites on the support surface during the activation process and 2. an alloy phase are created. This reduction behavior has a strong influence on the methanol conversion and selectivity results in the oxy-steam reforming of methanol reaction. It is well-known that copper catalysts with high Cu dispersion exhibit high activity in the reforming of methanol reaction.[4] It is also worth mentioning that an increase of the gold content in the copper supported catalyst caused the shift of the observed reduction effects to the higher temperature range. Additionally, in the case of the catalyst with the highest gold content, the occurrence of additional reduction stages connected with copper(II) oxychlorides and copper(II) chloride was observed at high temperature. It should be also emphasized that for all the studied catalyst systems the high temperature effect connected with the methanation process of the multi-walled carbon nanotubes was observed. Furthermore, in the case of the bimetallic Au–Cu supported catalysts, the observed high temperature effect can be also associated with the desorption of hydrogen chloride from the carbon material.

The reduction of bimetallic 3 wt% Au–Cu/CeO_2–ZrO_2 catalysts with various Au/Cu atomic ratios was studied by Pojanavaraphan *et al.*[32] who also observed the alloying process.

3.3. Phase composition studies of the bimetallic catalysts

To study the interactions between the active phase components and the support, the phase composition of the 5% Au–20% Cu/MWCNT (calcined, after reduction in a mixture of 5% H_2–95% Ar at 300 °C and the reaction) catalyst was investigated by the XRD technique. The results are given in Fig. 3. On the XRD diffractogram recorded for the bimetallic Au–Cu catalyst calcined at 180 °C, only a graphite-like phase corresponding to the MWCNTs, metallic gold and copper oxide phases was detected.

Yang *et al.*[36] studied the phase composition of reduced Cu/ZnO–CNT catalysts. Their XRD analysis showed diffraction peaks associated with CNT, Cu, CuO and ZnO in the XRD pattern. The CuO phase was visible in the diffraction curve because a portion of the metallic copper had been oxidized by oxygen in the air. Groβmann *et al.*[60] studied the phase composition of Cu/CNT catalysts and observed reflections coming from the monoclinic copper(II) oxide and a graphite-like phase, which is in agreement with our findings.

The phase composition results of the 5% Au–20% Cu/MWCNT catalyst after reduction at 300 °C in a reducing mixture of 5% H_2–95% Ar and the reaction are given also in Fig. 3. We observed that during the reduction process, an alloying process occurs. A confirmation of an alloying process between Au and Cu is the lack of diffraction peaks originating from the metallic gold phase in the case of catalysts containing 5 wt% gold. This finding was confirmed by the "*in situ*" XRD, TOF-SIMS and SEM-EDS results (see the next paragraphs).

Table 1 Temperature-programmed reduction (H_2-TPR) data for the monometallic copper catalyst after calcination in air for 4 h at 350 °C and the bimetallic Au–Cu/MWCNT catalysts after calcination in air for 4 h at 180 °C

	Peak contribution to the overall TPR peak area (%)			
Catalysts	LT-peak (T_{max1} = [°C])	HT-peak (T_{max2} = [°C])	Peak 3 (T_{max3} = [°C])	Peak 4 (T_{max4} = [°C])
20% Cu/MWCNT	32.5 (220)	67.5 (300)	—	—
0.5% Au–20% Cu/MWCNT	19.9 (205)	47.8 (245)	32.3 (265)	—
1% Au–20% Cu/MWCNT	17.1 (210)	31.7 (300)	51.2 (330)	—
5% Au–20% Cu/MWCNT	0.6 (230)	44.7 (325)	16.3 (350)	38.4 (430)

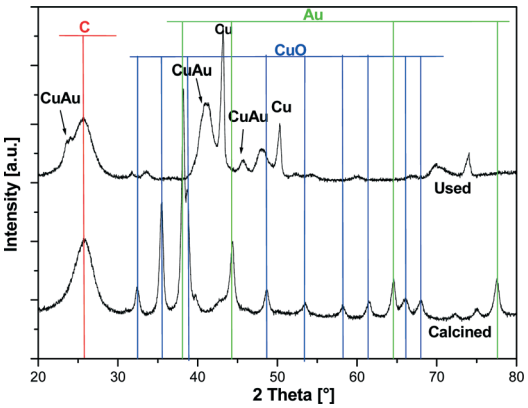

Fig. 3 XRD patterns of the calcined and used (after reduction at 300 °C in a mixture of 5% H_2–95% Ar and the reaction) bimetallic 5% Au–20% Cu/MWCNT catalysts.

To confirm the formation of an alloy between gold and copper, "*in situ*" XRD measurements were carried out. The temperature-programmed "*in situ*" XRD reduction measurements for the bimetallic 5% Au–20% Cu/MWCNT catalyst were carried out in a gas mixture of 5% H_2–95% Ar and the results are given in Fig. 4. The diffraction curves were collected in the temperature range from 50 to 800 °C. The phase composition analysis of the catalyst reduced at 50 °C confirmed the presence of the following crystallographic phases: Au, CuO and graphite-like phases. The XRD curve of the 5% Au–20% Cu/MWCNT system recorded at 200 °C showed in addition to the observed CuO, the diffraction peaks of the metallic gold and graphite-like phases positioned at 2theta = 36.42 and 42.30° assigned to the Cu_2O phase. The occurrence of these peaks confirmed the reduction mechanism of the CuO (CuO → Cu_2O → Cu) species through the intermediate Cu_2O. In order to better visualize the changes in the phase composition during the reduction of the 5% Au–20% Cu/MWCNT system, a fragment of the diffraction data collected in the 2theta angle = 35–45° in the temperature range of 50–600 C is shown in Fig. 4B. The diffraction curve recorded for the studied system showed clearly at 200 °C (see Fig. 4B) the appearance of the diffraction peaks of the Cu_2O phase. Increasing the reduction temperature up to 250 °C resulted in the appearance of the metallic phases of copper and gold in addition to the graphite-like structure. Further raising the temperature of the reduction up to 300 °C and higher causes an alloy Au–Cu formation.[65,70] Additionally, an increase of the reduction temperature above 250 °C causes an increase in the intensity of the diffraction peaks assigned to the metallic gold and metallic copper phases. The evidence of the solid solution formation is the shift of the main diffraction peak of Cu (111) (2theta = 43.30°) with an increase of the reduction temperature from 250 to 800 °C towards the lower values of the 2theta angle, which means that the unit cell increases as a result of the Au–Cu alloy formation. This is due to the fact that gold has a larger atomic radius than copper.[24] Additionally, the shift of the Au peak (111) (2theta = 38.34°) was also observed towards the lower values of the 2theta

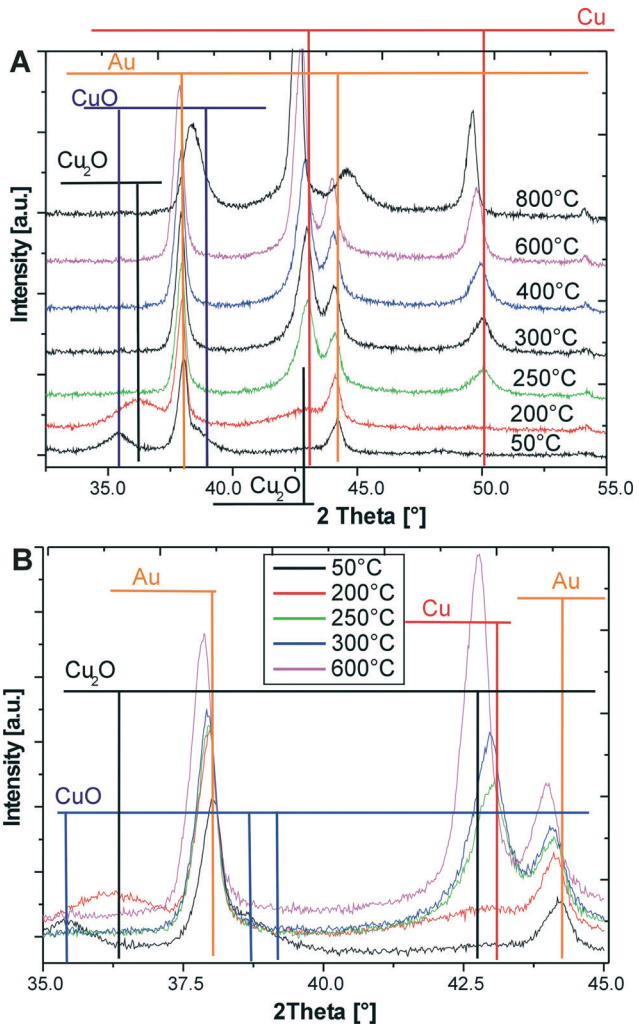

Fig. 4 XRD patterns collected for the bimetallic 5% Au–20% Cu/MWCNT catalyst during reduction in the temperature range of 50–800 °C in a mixture of 5% H_2–95% Ar.

angle. Similar results of the phase composition studies of bimetallic Au–Cu catalysts supported on a CeO_2–ZrO_2 mixed oxide prepared by the deposition–precipitation method were obtained by using XRD methods by Pojanavaraphan *et al.*[32]

The authors reported that the Au (111) diffraction peak observed on the diffraction pattern recorded for the Au/CeO_2–ZrO_2 catalysts was shifted towards the lower values of the 2theta angle from 38.34° to 38.17° in the presence of Cu loading. Additionally, this diffraction peak becomes broader in the case of the catalyst with a high copper loading. The authors associated the shift of the diffraction peak of the metallic copper phase with the formation of the Au–Cu alloy particles.

The application of copper–gold nanoparticles as a catalytic material was reported in ref. 71. The structure and behavior of the AuCu catalyst depend strongly on the preparation method. In the case of the catalyst prepared by a co-impregnation method reduced for 2 h in flowing hydrogen at 315 °C, electron X-ray absorption fine structure spectroscopy

(EXAFS) detected a degree of mixing between copper and gold. In contrast, the XRD results confirmed the migration of gold towards the core. Such core–shell structures were found in the case of the bimetallic alloy. The authors also reported that the copper–gold catalysts were more selective in acrolein synthesis from propene.

AuCu/TiO_2 alloy catalysts prepared by co-impregnation in the gas-phase epoxidation of propene by N_2O were also studied.[65] In these catalytic systems precise investigations performed by using XRD, XPS and transmission electron microscopy confirmed an AuCu alloy formation and a lattice parameter changing linearly with the CuAu ratio. They have found that the size of the alloy particle decreases together with the increase of the copper content in the investigated system.

Belin *et al.*[72] also studied the phase composition of CuAu/SiO_2 catalysts reduced in an H_2 atmosphere at 315 °C for 2 h prepared by an impregnation method for the selective oxidation of propene to acrolein. The authors reported that the reduction process causes the strong interaction between Cu and Au. The XRD analysis of the bimetallic Au–Cu catalysts confirmed AuCu species formation. The EXAFS results indicated copper–copper, copper–oxygen, copper–gold and gold–gold interactions. In addition, TEM measurements confirmed the inhomogeneous state of the catalyst surface. The catalytic activity of this system in the selective oxidation of propene to acrolein demonstrated a poor catalytic activity confirmed by a mixture of products obtained during the reaction. This mixture of products confirmed various active sites, which are present on the catalyst surface.

In our previous work,[24] we have done measurements for the Au–Cu reference material, similar to the supported Au–Cu/MWCNT catalyst weight ratio Au/Cu = 1 : 4 wt%. During the reduction process carried out for this reference material, we also observed the alloy formation, which takes place from 300 °C, which further confirms our results.

In the next step of the XRD studies, the composition of the AuCu alloy was calculated according to Vegard's law.[73,74] The resulting Au–Cu alloy is a solid solution with a cubic structure and therefore a linear combination of lattice spacing of the individual metal components and their mole fraction is given by the equation:

$$a_{CuAu} = X_{Au}a_{Au} + (1 - X_{Au})a_{Cu}$$

where a is the lattice constant and x is the mole fraction. Through the use of the lattice constant of pure Cu and that of the alloying atom (Au), the lattice constant of the remainder of the alloy compositions between 0 and 100 can be estimated using Vegard's law. The results of the lattice constant of an alloy and the mole fraction of gold in the catalytic material are shown in Table 2. Both Cu and Au are crystallized in the cubic system with space group $Fm\bar{3}m$.

To confirm the reduction mechanism of the Cu and Au–Cu catalysts, additional XRD measurements for the reduced catalysts were carried out and the results are shown in Fig. 5. A fragment of the diffraction data collected in the 2theta angle = 30–50° at a temperature of 220 and 300 °C for the monometallic copper catalyst is shown in Fig. 5A. The diffraction curve of the Cu/MWCNT system reduced at 220 °C showed only CuO and Cu_2O diffraction peaks, while the XRD diffraction curve of the monometallic copper catalyst reduced at 300 °C shows a diffraction peak that stem from the metallic copper phase. These results support the two-step reduction mechanism of CuO to metallic copper through a Cu_2O intermediate.

Table 2 Lattice constant (a) for the alloy and the mole fraction (x) for gold calculated for the system reduced at 250 and 800 °C

T [°C]	a_{CuAu} [Å]	x_{Au} [%]
250	3 615	0
800	3 652	7.98%

a_{Cu} = 36 150 [Å] PDF 004–0836, a_{Au} = 40 786 [Å] PDF 004–0784.

The phase composition results for the bimetallic 5% Au–20% Cu/MWCNT supported catalyst after reduction are given in Fig. 5B. The analysis of the diffraction curve obtained for the system reduced at 150 °C confirmed the occurrence of CuO, Cu_2O, $Cu_2(OH)_3Cl$ and metallic gold on a fragment of the diffraction curve recorded in Fig. 5B, while in the case of the bimetallic catalyst reduced at 300 °C, the XRD diffraction curve shows diffraction peaks that stem from the metallic copper, metallic gold and AuCu alloy phases. Additionally, it should be pointed out that the Au (111) diffraction peak which was observed on the diffraction pattern recorded for the Au–Cu/MWCNT catalyst reduced at 150 °C was shifted towards the lower values of 2theta in the case of the same catalyst reduced at 300 °C. This shift can be also explained in reference to the Au–Cu alloy formation.

Bracey *et al.*[75] also studied the phase composition of the bimetallic AuCu/SiO_2 catalysts after different thermal treatments.

An Au–Cu alloy formation in the case of the reduced bimetallic catalysts in a H_2–N_2 mixture at 315 °C was confirmed by XRD. The system obtained after reduction is very different and contains in its composition a copper–gold alloy. The XRD diffraction curve also shows the presence of some unalloyed gold, further confirmed by TEM-EDX. The alloy composition and structure depend strongly on the Cu and Au ratio in the catalytic material. The authors also reported that the copper–gold phase is very stable up to 675 °C and requires a high temperature to decompose to the copper oxide and metallic gold phases. It was found that the AuCu alloy requires a temperature between 650 and 800 °C in order to decompose to CuO and metallic Au. The formation of an alloy phase was confirmed also by visible spectroscopy, as the position of the plasmon peak shifts away from the position for gold with the changes in the copper–gold ratio.

3.4 SEM-EDS measurements

The 5% Au–20% Cu/MWCNT bimetallic catalyst was analyzed by scanning electron microscopy with X-ray microanalysis.

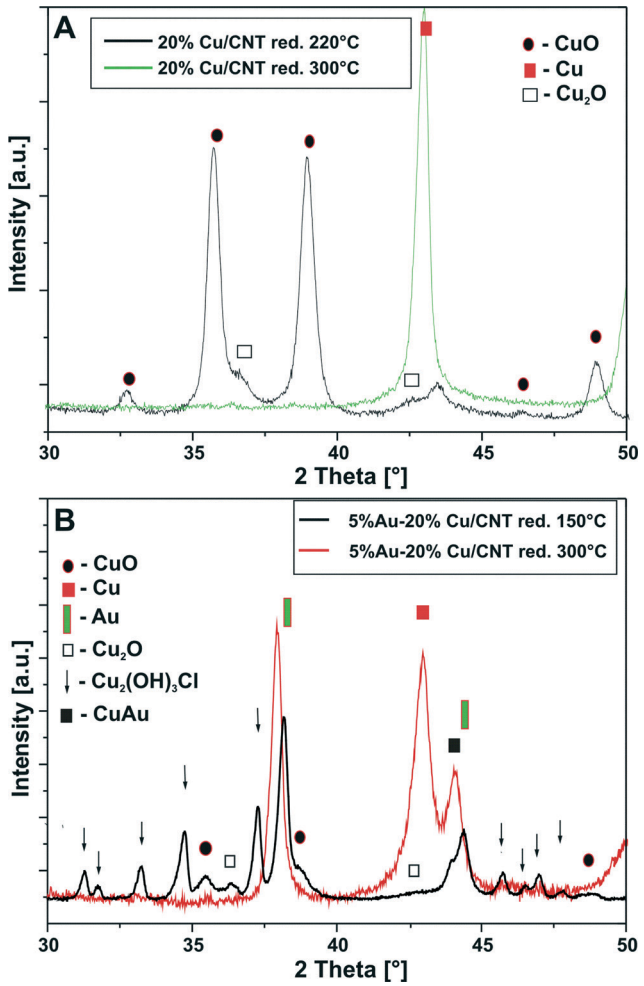

Fig. 5 (A) XRD patterns of the monometallic 20% Cu/MWCNT catalyst after being reduced in a mixture of 5% H_2–95% Ar at 220 and 300 °C. (B) Diffraction curves of the bimetallic 5% Au–20% Cu/MWCNT catalyst after being reduced in a mixture of 5% H_2–95% Ar at 150 and 300 °C in the range of 2θ (30–50°).

SEM-EDS was used to study the morphology and determine the surface composition of the MWCNT containing systems. Fig. 6 shows the SEM image obtained for the bimetallic 5% Au–20% Cu/MWCNT catalyst after being subjected to reduction and the reaction. Additionally, the studied catalyst was analyzed by EDS microanalysis. The numbers from 1 to 4 indicated the spots at which the EDS spectra were collected. The EDS results clearly showed that the catalyst's surface is not homogeneous as evidenced by the EDS spectra collected from the catalyst surface, which varied in elemental composition (see Fig. 6).

3.5 TOF-SIMS analysis

Secondary ion mass spectrometry was used to analyse the chemical status of the Au–Cu surface of the reference material, which contains the metals in an Au to Cu weight ratio = 1 : 4. Before the TOF-SIMS analysis, the reference sample was reduced in an atmosphere of 5% H_2–95% Ar at 300 °C.

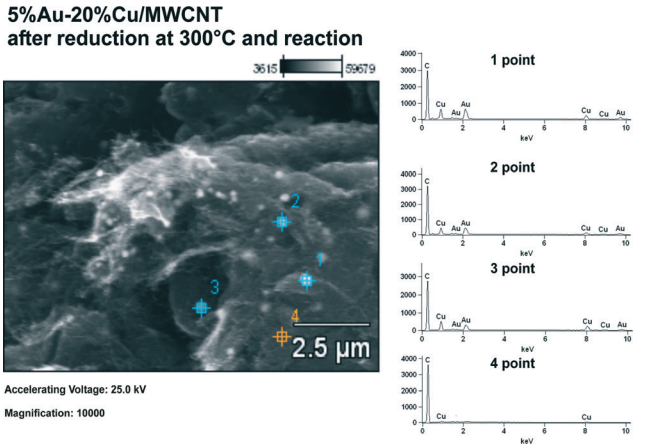

Fig. 6 EDS spectra and SEM image for the 5% Au–20% Cu/MWCNT catalyst after being reduced in a mixture of 5% H_2–95% Ar at 300 °C and the reaction.

Fig. 7A and B present fragments of the negative ion spectra. The analysis confirmed the presence of the secondary isotope copper–gold ions: $[^{63}CuAu]^-$ and $[^{65}CuAu]^-$ and the copper–gold–chlorine ions: $[^{63}CuAu^{35}Cl]^-$, $[^{65}CuAu^{35}Cl]^-$ or $[^{63}CuAu^{37}Cl]^-$ and $[^{65}CuAu^{37}Cl]^-$ on the surface. The presence of the $[^{63}CuAu]^-$ and $[^{65}CuAu]^-$ ions indicates the presence of the Au–Cu alloy on the catalyst surface, while the presence of the copper–gold–chlorine ($[^{63}CuAu^{35}Cl]^-$, $[^{65}CuAu^{35}Cl]^-$ or $[^{63}CuAu^{37}Cl]^-$ and $[^{65}CuAu^{37}Cl]^-$) ions on the negative ion spectrum confirmed the formation of the oxychlorides of copper(II) during the preparation process. The presence of these ions explains the shifts of the TPR profiles of the gold–copper catalyst towards the higher temperature range in comparison to the monometallic copper catalyst system.

3.6 Temperature-programmed desorption of ammonia.

The acidity of the prepared catalysts was studied using temperature-programmed desorption of ammonia.[76] TPD-NH_3 measurements were carried out to elucidate the effect of Au on the total acidity and define the role of the surface acidity on the catalytic reactivity in the oxy-steam reforming of methanol reaction.

The ammonia which is used as a probe molecule to study the properties of the acidic catalytic systems can interact with the surface of the studied material by physisorption or chemisorption processes through the lone pair of electron on its nitrogen atom.[77] The strength of the interaction which takes place between NH_3 and the investigated material depends on the electron accepting properties (*i.e.*, Lewis acidity).

The TPD-NH_3 profiles of the MWCNTs and the bimetallic supported catalysts calcined in an air atmosphere at 180 °C are shown in Fig. 8. The distribution of acid centers was also calculated based on the area under the peak situated at an appropriate desorption temperature and the results are given in Table 3. The temperature-programmed desorption profiles recorded for all the systems showed that all samples exhibited three kinds of acid centers *i.e.* weak, medium and

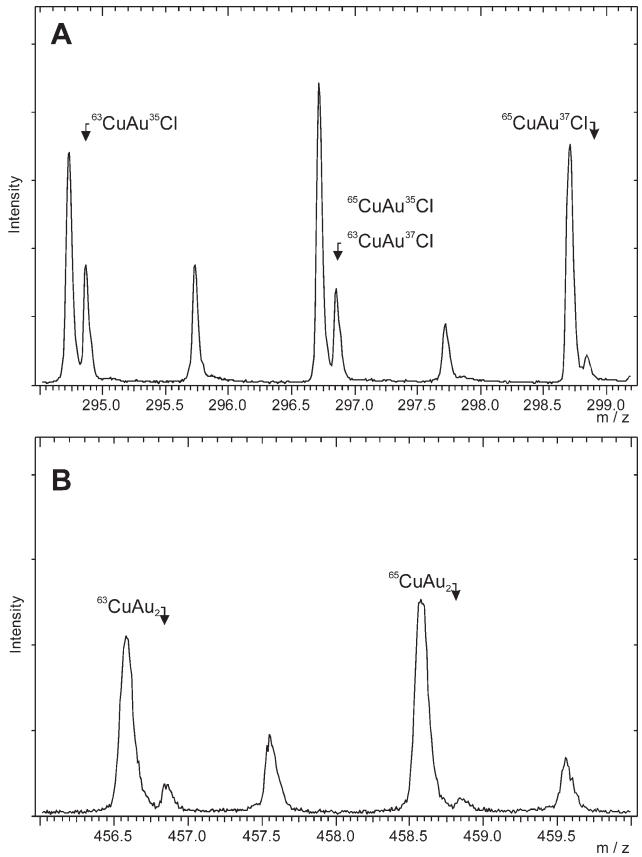

Fig. 7 TOF-SIMS spectra of the reference Au–Cu material containing the metals in an Au to Cu weight ratio of = 1:4 reduced in an atmosphere of 5% H_2–95% Ar at 300 °C.

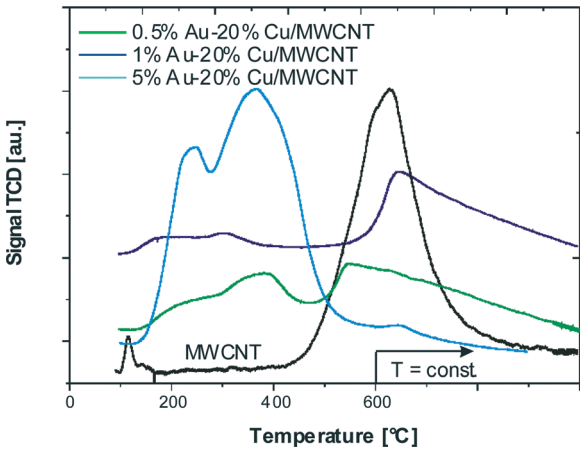

Fig. 8 TPD-NH_3 profile of the MWCNTs and bimetallic catalysts 1) 0.5% Au–20% Cu/MWCNT, 2) 1% Au–20% Cu/MWCNT, and 3) 5% Au–20% Cu/MWCNT after calcination in air for 4 h at 180 °C.

strong centers. The highest total acidity was shown by the multi-walled carbon nanotubes. The introduction of copper and gold into the MWCNTs caused a decrease in the total acidity. The highest acidity of all the catalyst systems calcined in air was shown by the catalyst containing the highest gold content.

Overall, the total acidity increased with an increase in the gold content. It is worth to note that in the case of the 5% Au–20% Cu/MWCNT catalyst, the participation of the weak and medium centers significantly increased the total acidity in comparison to the other bimetallic supported catalysts.

In the next step of our TPD-NH_3 investigation we studied the acidic properties of the catalytic systems after reduction in a mixture of 5% H_2–95% Ar at 300 °C in order to determine the influence of the acidic properties on the catalytic reactivity in the oxy-steam reforming of methanol. That is why we carried out the analogous TPD-NH_3 measurements for all the systems reduced "*in situ*" in a mixture of 5% H_2–95% Ar at 300 °C and the thermodesorption profiles are shown in Fig. 9. The distribution of the acid centres was also calculated for the reduced bimetallic catalysts and the results are given in Table 4. Also in the case of the reduced catalysts, three kinds of acidic centers were detected for all the systems, namely, weak acid, medium–strong and strong acid sites, which are present on the surface of each catalytic material.

The results obtained for our systems clearly showed that all the catalysts exhibited weak to strong electron accepting (Lewis acidic) properties. It is also worth to note that the 0.5% Au–20% Cu/MWCNT catalysts exhibited the highest acidity, which is also associated with the highest electron accepting properties. In addition, the 0.5% Au–20% Cu/MWCNT reduced catalytic system was characterized by the lowest concentration of the weak acid sites and exhibited the highest activity in the oxy-steam reforming of methanol. The TPD-NH_3 results of the reduced bimetallic catalysts indicate that an increase in the gold content in the investigated systems results in a decrease in the total acidity.

The intrinsic characteristics of the studied bimetallic Au–Cu catalysts such as the acid–base properties and density of the acid surface sites have a great influence on the catalytic performance of the catalyst in the oxy-steam reforming of methanol. It is well-known that the presence of the acid sites on the catalyst surface is fundamental for stabilizing intermediate species such as methoxy and formate.[78] These acidic properties may explain the differences in activity observed for all the studied catalysts in the oxy-steam reforming of methanol.

Pre-reduced Pd/CNT-promoted Cu–ZrO_2/HZSM-5 hybrid catalysts were prepared and their acidity was studied using the NH_3-TPD technique by Zhang *et al.*[79] The results from the TPD-NH_3 measurements carried out for CZ PdCNT/HZ, CZ CNT/HZ, CZ/HZ and HZSM-5 zeolites showed also three kinds of acid sites, which may be ascribed to the desorption of three kinds of NH_3-species adsorbed on the weak (mostly L-acid), medium–strong and strong acid (mostly B-acid) sites, respectively.

3.7 The influence of gold addition on the reactivity of the copper catalysts in the oxy-steam reforming of methanol reaction.

The oxy-steam reforming of methanol was also studied in this work. The results of the activity tests of the

Table 3 The amount of NH_3 adsorbed on the multi-walled carbon nanotubes and bimetallic catalysts calcined in an air atmosphere at 180 °C from the TPD-NH_3 data

Catalysts	Weak centers [μmol g^{-1}] 100–300 °C	Medium centers [μmol g^{-1}] 300–450 °C	Strong centers [μmol g^{-1}] 450–600 °C	Total acidity [μmol g^{-1}] 100–600 °C
MWCNT	143.7	42	652	837.7
0.5% Au–20% Cu/MWCNT	32.4	70.8	690.6	793.8
1% Au–20% Cu/MWCNT	35	21	676.4	732.4
5% Au–20% Cu/MWCNT	256.4	426	138.3	820.7

monometallic copper and bimetallic gold–copper supported catalysts in the OSRM reaction carried out at 200 °C and 300 °C expressed in methanol conversion and selectivity to hydrogen and the formation of carbon monoxide and carbon dioxide for all the studied catalytic systems are given in Fig. 10–12, respectively.

Fig. 10 shows the methanol conversion values for the mono- and bimetallic copper catalysts during the OSRM reaction at 200 and 300 °C. In the case of the 20% Cu/MWCNT catalyst, the conversion of methanol was 11% at 200 °C and increased as the temperature was raised. At 300 °C the consumption of methanol was 75%. Generally, the methanol conversion values for the mono- and bimetallic supported catalysts increased with temperature. By comparing the results of methanol conversion for the copper supported catalyst and the Au–Cu bimetallic catalysts it can be clearly seen that the promotion of the copper catalyst by gold slightly increases the methanol conversion at 200 °C, and far more distinctly at a temperature of 300 °C. It is worth noting that the highest increase in methanol conversion of 99.8% was achieved at 300 °C and was observed for the 0.5% Au–20% Cu/MWCNT catalyst.[80] The catalysts with a higher content of gold such as 1% Au–20% Cu/MWCNT and 5%–20% Cu/MWCNT showed methanol conversion at 300 °C at levels of 83 and 85%, respectively. It is worth to note that the methanol conversion increases together with the rise of the gold content in the catalytic systems at 200 °C. This means that the alloy phase formed during the activation process plays a crucial role during the oxy-steam reforming of methanol. The increase in activity can be explained by the creation of new centers of adsorption in the course of the reaction.

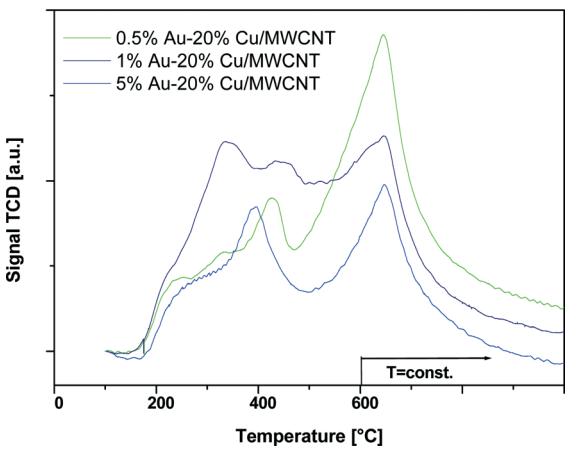

Fig. 9 TPD-NH_3 profile of the bimetallic catalysts 1) 0.5% Au–20% Cu/MWCNT, 2) 1% Au–20% Cu/MWCNT, and 3) 5% Au–20% Cu/MWCNT after calcination in air for 4 h at 180 °C and reduction in a mixture of 5% H_2–95% Ar at 300 °C.

Similar findings were reported by López *et al.*[64] They studied bimetallic CuNi/ZrO_2 catalysts in the OSRM and they have found that the high stability of the bimetallic catalysts is associated with the presence of the bimetallic Cu–Ni and core–shell Ni/Cu nanoparticles which are present on the support surface. They also claimed that the oxy-stem reforming of methanol may be a structure-sensitive reaction.

Bracey *et al.* also reported that an Au–Cu alloy created during the reduction process carried out at 315 °C was responsible for the activity improvement of the bimetallic Au–Cu/SiO_2 catalysts in propane oxidation.

At 300 °C the highest methanol conversion was shown by the 0.5% Au–20% Cu/MWCNT system and a further increase in the gold content in the catalytic material to 1% wt results in a decrease of the methanol conversion. However, a further increase in the gold content in the investigated system up to 5% wt of Au caused a slight increase of the methanol conversion. The activity results obtained in the oxy-steam reforming of methanol reaction demonstrate that the activity of the studied catalysts is not only connected with the gold content but also with the amount of the alloy phase in the investigated system. The catalytic tests confirmed that apart from the catalyst composition, other properties of the catalyst such as reducibility and acidity have a great influence on the catalytic activity of the investigated systems.

The highest activity (almost 100%) in the oxy-steam reforming of methanol in terms of methanol conversion was shown by the bimetallic catalysts containing the lowest content of gold. The observed reactivity results can be explained by the reductive properties and the acidic properties of the investigated system (electron accepting properties), and also by the presence of an alloy phase. The most active catalyst was the system reduced at the lowest temperature range (see Fig. 2 and Table 1). These results confirmed that in the case of this system we could expect the highest dispersion of metallic copper after the activation process is carried out at a temperature of 300 °C in a mixture of 5% H_2–95% Ar. The highest metallic copper dispersion could be explained by metal particles stemming from the copper oxide species, previously reduced at a low temperature range. On the other hand, the highest acidity indicates that the highest amount of the acid sites stabilizes the highest quantity of

Table 4 The amount of NH_3 adsorbed on the multi-walled carbon nanotubes and bimetallic catalysts calcined in an air atmosphere at 180 °C and reduced in a mixture of 5% H_2–95% Ar at 300 °C from the TPD-NH_3 data

Catalysts	Weak centers [μmol g^{-1}] 100–300 °C	Medium centers [μmol g^{-1}] 300–450 °C	Strong centers [μmol g^{-1}] 450–600 °C	Total acidity [μmol g^{-1}] 100–600 °C
0.5% Au–20% Cu/MWCNT	68.1	153.2	706.4	927.8
1% Au–20% Cu/MWCNT	97.8	247.3	519.3	864.4
5% Au—20% Cu/MWCNT	61.7	153.4	344.8	559.9

intermediates during the reaction, which are further dehydrated and dehydrogenated into the main products (CO_2 and H_2). This can also explain the highest activity of this catalyst.

In summary, the methanol conversion results indicate that the value of methanol conversion depends strongly on the quantity of the alloy phase, which is also an active center during the reaction. In addition, the present results indicate that the reducibility of each system and the acidic properties are also important factors influencing the catalyst reactivity.

The H_2 yield is shown in Fig. 11 for all the catalysts at 200 and 300 °C. The results of the hydrogen yield obtained at 200 °C showed an opposite trend in comparison to the methanol conversion for all the catalysts. The H_2 yield decreases together with the increase in the gold content in the bimetallic system. While at 300 °C, the H_2 yield generally parallels the methanol conversion.

The higher yield of hydrogen was shown by the 0.5% Au–20% Cu/MWCNT bimetallic catalyst, which also was the most active system at 300 °C. The increase of the gold content in the bimetallic catalyst results in a decrease in the H_2 yield during the reaction which is in good agreement with the acidity results showing a decrease in the total acidity with an increase in the gold content.

Fig. 12 shows the selectivity results towards carbon monoxide and carbon dioxide formations obtained in the tested reaction. The selectivity results obtained at 200 °C showed no carbon monoxide formation. No CO formation was observed during the reaction carried out at 200 °C. This result can be easily explained because CO is a by-product of the methanol decomposition and reverse water-gas shift endothermic reactions. Increasing the reaction temperature to 300 °C led to the appearance of carbon monoxide in the reaction products. The lowest quantity of carbon monoxide in the reaction products was obtained at 300 °C, which was exhibited by the copper catalyst and the 1% Au–20% Cu/MWCNT system. The promotion of the copper catalyst by gold leads to a decrease in selectivity towards carbon dioxide and an increase in selectivity towards CO. These results can be explained by the fact that at a higher reaction temperature (300 °C) both the methanol oxy-steam reforming and reverse water gas shift reactions (RWGS) run at the same time. This is evidenced by the formation of carbon monoxide and the decrease in selectivity towards CO_2. In contrast, when the OSRM is performed at a low temperature (200 °C), increasing the metal content in the catalytic material caused the increase in methanol conversion and the reaction of the oxy-stem reforming of methanol to proceed more easily.[56]

The catalytic activity measurements carried out for all the catalysts showed that gold played a positive role on the activity of the studied catalysts. This is evidenced by the methanol conversion values of the bimetallic supported catalysts which were all higher compared to the monometallic copper catalysts. The promotion effect on the H_2 yield was also proven in the case of the bimetallic catalysts. It is also worth to note that the highest activity and yield of H_2 formation was exhibited by the catalyst with the highest electron accepting properties which was the easiest reducible system compared to the other investigated systems.

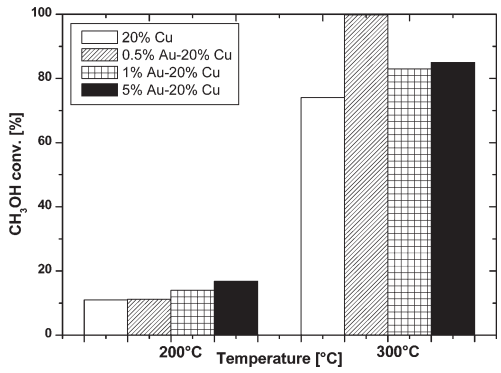

Fig. 10 Effect of the temperature on the methanol conversion in the oxy-steam reforming of methanol over the mono- and bimetallic catalysts supported on MWCNT. Reaction conditions: $H_2O/CH_3OH/O_2$ = 1/1/0.4, GHSV = 2.67×10^4 h^{-1}.

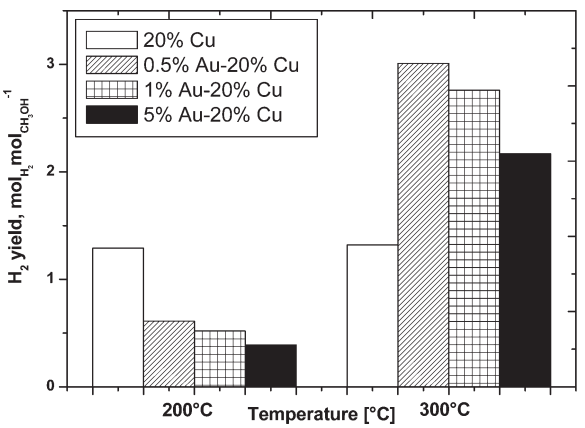

Fig. 11 H_2 yield as a function of temperature in the oxy-steam reforming of methanol. Reaction conditions: $H_2O/CH_3OH/O_2$ = 1/1/0.4, GHSV = 2.67×10^4 h^{-1}.

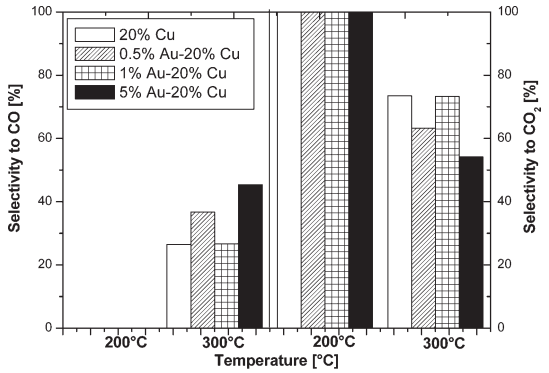

Fig. 12 Results of the selectivity to the carbon monoxide and carbon dioxide formations in the oxy-steam reforming of methanol over the monometallic copper and bimetallic Au–Cu catalysts supported on MWCNTs. Reaction conditions: $H_2O/CH_3OH/O_2$ = 1/1/0.4, GHSV = 2.67×10^4 h^{-1}.

Cu/ZnO and $Cu/ZnO/Al_2O_3$ catalysts[22] were studied in the oxy-steam reforming of methanol. The reactivity results showed that methanol conversion increases with the reaction temperature according to typical S shaped curves. At 200 °C the methanol conversion reached the maximum value of about 18% for the $Cu/ZnO/Al_2O_3$ catalyst (metal composition (at%) Cu = 18, Zn = 33, Al = 49). In contrast, for the rest of the catalysts the reaction does not proceed at 200 °C, while at the reaction temperature of 300 °C, the methanol conversion for the same catalyst was about 82%. This value was lower for the other systems with higher and lower copper contents. For all the catalysts, the methanol conversion reached 100% at a temperature of 350–400 °C. These results gave evidence that there is no simple correlation between the activity and the copper content or copper area in the catalyst system. This means that the activity of the copper catalysts depends on the other properties of the investigated system. The yield of hydrogen for all the catalysts parallels the methanol conversion at a given temperature. The highest H_2 yield was obtained for the catalyst which showed the highest methanol conversion. However, the hydrogen yield decreases at high temperature. At high reaction temperatures (350–400 °C), the highest H_2 yield was exhibited by the $Cu/ZnO/Al_2O_3$ catalysts containing the lowest concentration of copper (metal composition (at%) Cu = 5, Zn = 50, Al = 45). In this work, we also found similar findings for the activity results obtained for the conventional Cu/ZnO or $Cu/ZnO/Al_2O_3$ catalysts obtained in ref. 22.

We also confirmed that the bimetallic Au–Cu/MWCNT catalytic systems showed the same or even higher methanol conversion at 300 °C compared to the conventional catalysts studied by Turco *et al.*[22] In addition, the H_2 yield obtained for the 0.5% Au–20% Cu/MWCNT catalyst was higher than in the case of the conventional $Cu/ZnO/Al_2O_3$ catalyst but exhibited lower selectivity to CO formation.

Hereijgers *et al.*[78] investigated a series of basic metal oxide-promoted gold catalysts (Au/Al_2O_3, Au/La_2O_3, $AuMO_x/Al_2O_3$, where M = Mg, Ca, Sr, Ba, La) in the partial oxidation of methanol reaction in order to produce CO-free hydrogen. The activity tests performed for the promoted catalysts showed that the selectivity towards the formation of hydrogen increases with increasing basicity of the alkaline earth metal oxide which was added to the catalytic system. The selectivity to hydrogen production increases in the following order: unpromoted catalyst < MgO < CaO < SrO < BaO. However, the selectivity results towards CO and CH_4 formations showed an opposite trend.

It has been reported that Au nanoparticles on a La_2O_3 support exhibited superior catalytic performance in terms of H_2 production and suppressing CO formation. These results were explained by the promoting effect of the acid/base properties of the support which reduce the occurrence of undesired reactions, *e.g.*, methanation and the formation of carbon monoxide.[78]

In the same work,[78] the authors compared their catalytic systems with commercial catalysts like the Cu/ZnO system in the partial oxidation of methanol reaction carried out at 300 °C. Their catalytic system showed an even higher methanol conversion of above 85% for the $AuLa_2O_3/Al_2O_3$ system in comparison to the commercial catalysts which exhibited a methanol conversion of about 82%. On the other hand, the commercial catalyst showed the highest hydrogen selectivity of 98% but the selectivity towards CO was only 12%. It is worth to note that the gold catalyst supported on La_2O_3 showed a lower methanol conversion (54%) in the studied reaction and also the lowest selectivity towards the formation of carbon monoxide (2.1%). At the same time, no methane formation was observed on this catalyst.

Monometallic copper Cu/ZrO_2, nickel Ni/ZrO_2 and bimetallic $Cu/Ni/ZrO_2$ catalysts prepared by a deposition–precipitation method were also studied in the oxy-steam reforming of methanol in the temperature range of 250–360 °C by Pérez-Hernández *et al.*[81] The reactivity results in the oxy-steam reforming of methanol showed that the main products of the reaction performed using the bimetallic catalysts were H_2, CO, CO_2 and H_2O. A trace of methyl formate and methane in the product mixture of the reaction was observed. The bimetallic catalysts showed the best catalytic performance in the OSRM at a low temperature range. On the other hand, the Ni supported catalyst was more effective compared to the Cu catalyst at high temperature. All the tested catalysts exhibited the same selectivity towards H_2 at 360 °C, which was about 60%. The high selectivity towards CO is explained by the presence of Ni-rich bimetallic nanoparticles, the existence of which was confirmed by TEM and EDX analyses.

Conclusions

This work provides evidence that gold promotion of copper catalysts has a significant impact on the activity and selectivity of the copper catalysts in the oxy-steam reforming of methanol. It was found that the Au–Cu alloy is formed during the reduction process carried out at 300 °C. The occurrence of this alloy was confirmed by the "*in situ*" XRD

measurements, TOF-SIMS and SEM-EDS techniques. It was also found that the Au–Cu alloy formed during the activation process was the active phase in the oxy-steam reforming of methanol. It was also demonstrated that the acidity (electron accepting properties) and reducibility of the investigated systems have an influence on the activity of the tested catalysts in the studied reaction. The highest activity and H_2 yield were shown by the 0.5% Au–20% Cu/MWCNT bimetallic catalyst which had the highest total acidity and was the easiest reducible system compared to the other investigated systems. It was also found that an increase in the total acidity increased the methanol conversion value and H_2 yield for the investigated bimetallic catalysts. This tendency can be explained by fact that the acidic sites stabilize the intermediate formed during the reaction. The facilitated reduction and thermal decomposition of the copper catalysts supported on the multiwalled carbon nanotubes after gold promotion were proven by the TG and TPR-H_2 techniques. The activity results confirm the possibility of the use of the investigated materials for H_2 generation by the oxy-steam reforming of methanol.

Acknowledgements

The project was funded by the National Science Centre (Grant no. DEC 2012/05/D/ST8/02856).

Notes and references

1 S.-C. Yang, W.-N. Su, S. D. Lin, J. Rick and B.-J. Hwang, *Catal. Sci. Technol.*, 2012, **2**, 807–812.
2 J.-P. Shen and C. Song, *Catal. Today*, 2002, **77**, 89–98.
3 J. Kuc, M. Neumann, M. Armbruster, S. Yoon, Y. Zhang, R. Erni, A. Weidenkaff and S. K. Matam, *Catal. Sci. Technol.*, 2016, DOI: 10.1039/c5cy01410g.
4 C. Mateos-Pedrero, H. Silva, D. A. Pacheco Tanaka, S. Liguori, A. Iulianelli, A. Basile and A. Mendes, *Appl. Catal., B*, 2015, **174–175**, 67–76.
5 J. Wang, C.-H. Li and T.-J. Huang, *Catal. Lett.*, 2005, **103**, 239–247.
6 W. Shan, Z. Feng, Z. Li, J. Zhang, W. Shen and C. Li, *J. Catal.*, 2004, **228**, 206–217.
7 S. Patel and K. K. Pant, *Fuel Process. Technol.*, 2007, **88**, 825–832.
8 J. Papavasiliou, G. Avgouropoulos and T. Ioannides, *Catal. Commun.*, 2004, **5**, 231–235.
9 T. Shishido, Y. Yamamoto, H. Morioka and K. Takehira, *J. Mol. Catal. A: Chem.*, 2007, **268**, 185–194.
10 L. Yong-Feng, D. Xin-Fa and L. Wei-Ming, *Int. J. Hydrogen Energy*, 2004, **29**, 1617–1621.
11 I. Ritzkopf, S. Vukojević, C. Weidenthaler, J.-D. Grunwaldt and F. Schüth, *Appl. Catal., A*, 2006, **302**, 215–223.
12 C.-T. Wang and R. J. Willey, *Catal. Today*, 1999, **52**, 83–89.
13 T. Shishido, Y. Yamamoto, H. Morioka, K. Takaki and K. Takehira, *Appl. Catal., A*, 2004, **263**, 249–253.
14 Y. Matsumura, K. Tanaka, N. Tode, T. Yazawa and M. Haruta, *J. Mol. Catal. A: Chem.*, 2000, **152**, 157–165.
15 S. Liu, K. Takahashi, K. Uematsu and M. Ayabe, *Appl. Catal., A*, 2005, **283**, 125–135.
16 H. Jeong, K. I. Kim, T. H. Kim, C. H. Ko, H. C. Park and I. K. Song, *J. Power Sources*, 2006, **159**, 1296–1299.
17 J. Papavasiliou, G. Avgouropoulos and T. Ioannides, *J. Catal.*, 2007, **251**, 7–20.
18 L. Ma, B. Gong, T. Tran and M. S. Wainwright, *Catal. Today*, 2000, **63**, 499–505.
19 P. Clancy, J. P. Breen and J. R. H. Ross, *Catal. Today*, 2007, **127**, 291–294.
20 C.-Z. Yao, L.-C. Wang, Y.-M. Liu, G.-S. Wu, Y. Cao, W.-L. Dai, H.-Y. He and K.-N. Fan, *Appl. Catal., A*, 2006, **297**, 151–158.
21 O. Jakdetchai, N. Takayama and T. Nakajima, *Kinet. Catal.*, 2005, **46**, 56–64.
22 M. Turco, G. Bagnasco, C. Cammarano, P. Senese, U. Costantino and M. Sisani, *Appl. Catal., B*, 2007, **77**, 46–57.
23 M. Haruta, N. Yamada, T. Kobayashi and S. Iijima, *J. Catal.*, 1989, **115**, 301–309.
24 P. Mierczynski, T. Maniecki, W. Maniukiewicz and W. Jozwiak, *React. Kinet., Mech. Catal.*, 2011, **104**, 139–148.
25 T. Maniecki, P. Mierczynski, W. Maniukiewicz, K. Bawolak, D. Gebauer and W. Jozwiak, *Pol. J. Chem.*, 2008, **82**, 2379–2388.
26 T. Maniecki, P. Mierczynski, K. Bawolak, D. Gebauer, W. Maniukiewicz and W. Jozwiak, *Pol. J. Chem.*, 2008, **82**, 2367–2378.
27 T. Maniecki, P. Mierczynski, W. Maniukiewicz, K. Bawolak, D. Gebauer and W. Jozwiak, *Catal. Lett.*, 2009, **130**, 481–488.
28 C. W. Corti, R. J. Holliday and D. T. Thompson, *Appl. Catal., A*, 2005, **291**, 253–261.
29 T. Maniecki, K. Bawolak, P. Mierczynski and W. Jozwiak, *Catal. Lett.*, 2009, **128**, 401–404.
30 T. Maniecki, K. Bawolak-Olczak, P. Mierczynski, W. Maniukiewicz and W. Jozwiak, *Chem. Eng. J.*, 2009, **154**, 142–148.
31 T. Tabakova, G. Avgouropoulos, J. Papavasiliou, M. Manzoli, F. Boccuzzi, K. Tenchev, F. Vindigni and T. Ioannides, *Appl. Catal., B*, 2011, **101**, 256–265.
32 C. Pojanavaraphan, A. Luengnaruemitchai and E. Gulari, *Appl. Catal., A*, 2013, **456**, 135–143.
33 C. Pojanavaraphan, A. Luengnaruemitchai and E. Gulari, *Int. J. Hydrogen Energy*, 2012, **37**, 14072–14084.
34 C. Pojanavaraphan, A. Luengnaruemitchai and E. Gulari, *Chem. Eng. J.*, 2012, **192**, 105–113.
35 C. Pojanavaraphan, U. Satitthai, A. Luengnaruemitchai and E. Gulari, *J. Ind. Eng. Chem.*, 2015, **22**, 41–52.
36 H.-M. Yang and P.-H. Liao, *Appl. Catal., A*, 2007, **317**, 226–233.
37 P.-H. Liao and H.-M. Yang, *Catal. Lett.*, 2008, **121**, 274–282.
38 M. Turco, G. Bagnasco, U. Costantino, F. Marmottini, T. Montanari, G. Ramis and G. Busca, *J. Catal.*, 2004, **228**, 43–55.
39 T. Maniecki, A. Stadnichenko, W. Maniukiewicz, K. Bawolak, P. Mierczynski, A. Boronin and W. Jozwiak, *Kinet. Catal.*, 2010, **51**, 573–578.
40 T. Maniecki, K. Bawolak, D. Gebauer, P. Mierczynski and W. Jozwiak, *Kinet. Catal.*, 2009, **50**, 138–144.

41 J. Zhao, J. Xu, J. Xu, T. Zhang, X. Di, J. Ni and X. Li, *Chem. Eng. J.*, 2015, **262**, 1152–1160.
42 T.-C. Ou, F.-W. Chang and L. S. Roselin, *J. Mol. Catal. A: Chem.*, 2008, **293**, 8–16.
43 A. Sandoval, C. Louis and R. Zanella, *Appl. Catal., B*, 2013, **140–141**, 363–377.
44 N. K. Gamboa-Rosales, J. L. Ayastuy, M. P. González-Marcos and M. A. Gutiérrez-Ortiz, *Int. J. Hydrogen Energy*, 2012, **37**, 7005–7016.
45 X. Liao, W. Chu, X. Dai and V. Pitchon, *Appl. Catal., B*, 2013, **142–143**, 25–37.
46 X. Liu, A. Wang, L. Li, T. Zhang, C.-Y. Mou and J.-F. Lee, *J. Catal.*, 2011, **278**, 288–296.
47 P. K. Seelam, M. Huuhtanen, A. Sápi, M. Szabó, K. Kordás, E. Turpeinen, G. Tóth and R. L. Keiski, *Int. J. Hydrogen Energy*, 2010, **35**, 12588–12595.
48 C. Pham-Huu, N. Keller, G. Ehret, L. C. J. Charbonniere, R. Ziessel and M. J. Ledoux, *J. Mol. Catal. A: Chem.*, 2001, **170**, 155–163.
49 T. Hou, L. Yuan, T. Ye, L. Gong, J. Tu, M. Yamamoto, Y. Torimoto and Q. Li, *Int. J. Hydrogen Energy*, 2009, **34**, 9095–9107.
50 A. Solhy, B. F. Machado, J. Beausoleil, Y. Kihn, F. Gonçalves, M. F. R. Pereira, J. J. M. Órfão, J. L. Figueiredo, J. L. Faria and P. Serp, *Carbon*, 2008, **46**, 1194–1207.
51 J.-P. Tessonnier, L. Pesant, G. Ehret, M. J. Ledoux and C. Pham-Huu, *Appl. Catal., A*, 2005, **288**, 203–210.
52 V. M. Shinde, E. Skupien and M. Makkee, *Catal. Sci. Technol.*, 2015, **5**, 4144–4153.
53 C. Zhou, Y. Chen, Z. Guo, X. Wang and Y. Yang, *Chem. Commun.*, 2011, **47**, 7473–7475.
54 P. Sangeetha, L.-H. Chang and Y.-W. Chen, *Mater. Chem. Phys.*, 2009, **118**, 181–186.
55 E. Mosquera, D. E. Diaz-Droguett, N. Carvajal, M. Roble, M. Morel and R. Espinoza, *Diamond Relat. Mater.*, 2014, **43**, 66–71.
56 P. Mierczynski, R. Ciesielski, A. Kedziora, M. Nowosielska, J. Kubicki, W. Maniukiewicz, A. Czylkowska and T. Maniecki, *React. Kinet., Mech. Catal.*, 2015, 1–17.
57 P. Mierczynski, K. Vasilev, A. Mierczynska, W. Maniukiewicz, M. I. Szynkowska and T. P. Maniecki, *Appl. Catal., B*, 2016, **185**, 281–294.
58 N. Mahata, O. S. G. P. Soares, I. Rodríguez-Ramos, M. F. R. Pereira, J. J. M. Órfão and J. L. Figueiredo, *Appl. Catal., A*, 2013, **464–465**, 28–34.
59 S. Song and S. Jiang, *Appl. Catal., B*, 2012, **117–118**, 346–350.
60 D. Großmann, A. Dreier, C. W. Lehmann and W. Grünert, *Microporous Mesoporous Mater.*, 2015, **202**, 189–197.
61 N. Pasupulety, H. Driss, Y. A. Alhamed, A. A. Alzahrani, M. A. Daous and L. Petrov, *Appl. Catal., A*, 2015, **504**, 308–318.
62 C.-X. Sun, Y. Wang, A.-P. Jia, S.-X. Chen, M.-F. Luo and J.-Q. Lu, *J. Catal.*, 2014, **312**, 139–151.
63 C. Kartusch and J. van Bokhoven, *Gold Bull.*, 2009, **42**, 343–348.
64 P. López, G. Mondragón-Galicia, M. E. Espinosa-Pesqueira, D. Mendoza-Anaya, M. E. Fernández, A. Gómez-Cortés, J. Bonifacio, G. Martínez-Barrera and R. Pérez-Hernández, *Int. J. Hydrogen Energy*, 2012, **37**, 9018–9027.
65 R. J. Chimentão, F. Medina, J. L. G. Fierro, J. Llorca, J. E. Sueiras, Y. Cesteros and P. Salagre, *J. Mol. Catal. A: Chem.*, 2007, **274**, 159–168.
66 S. Pongstabodee, S. Monyanon and A. Luengnaruemitchai, *J. Ind. Eng. Chem.*, 2012, **18**, 1272–1279.
67 H.-C. Yang, F.-W. Chang and L. S. Roselin, *J. Mol. Catal. A: Chem.*, 2007, **276**, 184–190.
68 E. D. Guerreiro, O. F. Gorriz, J. B. Rivarola and L. A. Arrúa, *Appl. Catal., A*, 1997, **165**, 259–271.
69 B. Lindström, L. J. Pettersson and P. Govind Menon, *Appl. Catal., A*, 2002, **234**, 111–125.
70 W. Li, A. Wang, X. Liu and T. Zhang, *Appl. Catal., A*, 2012, **433–434**, 146–151.
71 C. L. Bracey, P. R. Ellis and G. J. Hutchings, *Chem. Soc. Rev.*, 2009, **38**, 2231–2243.
72 S. Belin, C. L. Bracey, V. Briois, P. R. Ellis, G. J. Hutchings, T. I. Hyde and G. Sankar, *Catal. Sci. Technol.*, 2013, **3**, 2944–2957.
73 C. G. Sonwane, J. Wilcox and Y. H. Ma, *J. Phys. Chem. B*, 2006, **110**, 24549–24558.
74 P. Mierczynski, K. Vasilev, A. Mierczynska, W. Maniukiewicz and T. P. Maniecki, *Appl. Catal., A*, 2014, **479**, 26–34.
75 C. L. Bracey, A. F. Carley, J. K. Edwards, P. R. Ellis and G. J. Hutchings, *Catal. Sci. Technol.*, 2011, **1**, 76–85.
76 P. Mierczynski, K. A. Chalupka, W. Maniukiewicz, J. Kubicki, M. I. Szynkowska and T. P. Maniecki, *Appl. Catal., B*, 2015, **164**, 176–183.
77 H. N. Hareesh, K. U. Minchitha, N. Nagaraju and N. Kathyayini, *Chin. J. Catal.*, 2015, **36**, 1825–1836.
78 B. P. C. Hereijgers and B. M. Weckhuysen, *ChemSusChem*, 2009, **2**, 743–748.
79 M.-H. Zhang, Z.-M. Liu, G.-D. Lin and H.-B. Zhang, *Appl. Catal., A*, 2013, **451**, 28–35.
80 A. Gazsi, I. Ugrai and F. Solymosi, *Appl. Catal., A*, 2011, **391**, 360–366.
81 R. Pérez-Hernández, G. Mondragón Galicia, D. Mendoza Anaya, J. Palacios, C. Angeles-Chavez and J. Arenas-Alatorre, *Int. J. Hydrogen Energy*, 2008, **33**, 4569–4576.